Experimental Investigation of a Dynamically Forced Impinging Jet Array

Frank Haucke and Arne Berthold

Abstract Dynamic forced impingement cooling is investigated experimentally. Due to the pulsation of impinging jets, strong ring vortices can be generated. Thereby, pulse parameters, e.g. frequency, amplitude, duty cycle and phase shift as well as geometrical parameters e.g. impingement distance, jet nozzle distance or jet nozzle arrangement, play an important role on maximizing the heat transfer on hot surfaces. In the present paper the local convective heat transfer on an electrically heated flat plate is being investigated, while under the influence of a 7 by 7 inline impinging jet array. The cooling efficiency of pulsed actuation with side wall induced crossflow is determined by comparing local Nusselt numbers to the steady blowing case.

Keywords Heat transfer · Impingement cooling · Dynamic forcing
Pulsed blowing · Crossflow · Experimental

1 Introduction

It is the vision of the Collaborative Research Center "SFB1029" to enhance the overall efficiency of the real gas turbine process by more than 10%. By employing classical design methods based on constant-pressure combustion only marginal improvements can be expected in the future. Thus, the focus is on constant-volume combustion, which generally promises significant efficiency increase from a thermodynamic point of view. As a result of this strategy, the combustion process would be highly unsteady, which is induced by classical pulsed detonation or by a new shockless explosion concept. In this scenario, periodic pressure and temperature changes originated within the combustion chamber occur that influence the flow

F. Haucke (✉) · A. Berthold
Technische Universität Berlin, Department of Aeronautics and Astronautics,
Chair of Aerodynamics, Marchstreet 12–14, 10587 Berlin, Germany
e-mail: Frank.Haucke@ilr.tu-berlin.de

A. Berthold
e-mail: Arne.Berthold@tu-berlin.de

characteristics of all gas turbine components. With respect to the first turbine stage a significant increased heat load is expected. Modern turbine cooling strategies are based on the combination of high-temperature proved super alloy materials, film cooling and internal cooling concepts. Impingement cooling is an effective convective cooling method that provides high local heat transfer rates inside turbine blades. After impinging on the hot inner surface, the cooling air mass flow is directed to the trailing edge and is discharged to the main hot gas flow. Thereby, upstream jets generate a cross flow that superimposes downstream impinging jets.

The geometrical configuration, including hole diameter, hole spacing, hole arrangement and impingement distance as well as the local Reynolds number of the cooling air mass flow, has a significant impact on local heat transfer, which was experimentally investigated in-depth by Florschuetz et al. [1, 2], Weigand and Spring [3] and Xing et al. [4].

One fundamental goal of industrial gas turbine development is a high efficient exploitation of cooling air mass flow. The active excitation of impinging jets could be a promising way to increase local heat transfer in the impinging zone. Liu and Sullivan [5] and Vejrazka et al. [6] experimentally investigated a single impinging jet under excitation. At normalized nozzle to plate distances lower than $S/D \leq 2$, forcing of the impinging jet has a high potential to affect the heat transfer in the wall jet region. However, heat transfer within the stagnation area is almost uninfluenced.

Hofmann et al. [7] found that the interaction between jet and environment can cause an intensified mixing, which reduces the jet velocity. Thus, heat transfer can be reduced especially for large nozzle to plate distances. The mixing effect is reduced for smaller impingement distances. If the Strouhal number is in the order of turbulence magnitude, heat transfer can be enhanced. Thereby, a threshold Strouhal number of $Sr_D = 0.2$ was determined.

Gahrib et al. [8] describes the generation of high energy ring vortices. The "formation number" t^* was introduced and limits were defined for the production of ring vortices with maximized size, vorticity and amplitude. In this context Herwig et al. [9] and Middleberg et al. [10] describe the production of very strong vortices using square pulses. This enforces periodically strong local and temporal velocity gradients and thus maximize local convective heat transfer. These facts were corroborated by the findings of Janetzke et al. [11]. Influenced by the actuator characteristic there is a dependency between the enhancement of local Nusselt number and the combination of Strouhal number and amplitude. The field of combination of geometrical and dynamic parameters is very large. The characteristics of an actuation system plays an important role as well. Thereby, the impact of dynamically forced impinging jets on the local heat transfer in the stagnation zone and in the wall jet zone is not fully discovered yet.

The present study is focused on further experimental investigation of the local convective heat transfer of an array of 7 by 7 dynamically forced impinging jets [12]. In particular, interactions between adjacent impinging jets and their accompanying vortex structures is of special interest for dynamic heat transfer issues.

2 Experimental Set-Up

In Fig. 1 the basic test rig geometry is schematically displayed. It allows the systematic investigation of the heat transfer on a flat plate as well as the study of the velocity flow field under a 7 by 7 impinging jet array. The jet nozzle dimensions are equivalent to those of Janetzke [11]. Furthermore, the geometry is equivalent to a simple drill hole, with an diameter of $D = 12$ mm and a length over diameter ratio of $L/D = 2.5$. The basic normalized spacing between two nozzles is $S/D = 5$.

The air mass flow, which passes through each nozzle, is supplied by a standard in-house compressed air system. In order to provide the desired amount of air, four mass flow control units are used. Each unit consists of an electronic, proportional pressure regulator and an electronic mass flow controller. Both components are connected in series. Downstream of these components, one air flow divider is connected to each mass flow control unit and feeds up to 13 nozzles. In case of investigating pulsed impinging jets, one fast switching valve is added upstream of each nozzle. The standard valve parameters are as follows: maximum normalized volume flow rate: $V_N = 160 l_N/min$, the maximum switching frequency: $f_{max} = 500$ Hz.

Heat transfer apparatus: Liquid crystal thermography (LCT) was employed to determine the two dimensional distribution of Nusselt numbers in the impingement area under steady state and dynamically forced flow conditions. The corresponding schematic LCT arrangement is presented in Fig. 2. The impingement plate is a transparent glass plate with the dimensions 1 m × 1 m × 12 mm. It provides optical access into the testing area and therefore allows a high degree of flexibility in two-dimensional temperature measurements employing liquid crystal thermography.

The LCT foil is of type Hallcrest "R30C5W" and has an self adhesive backing, which is used to attach it to a thin steel foil. The dimensions of this steel foil are
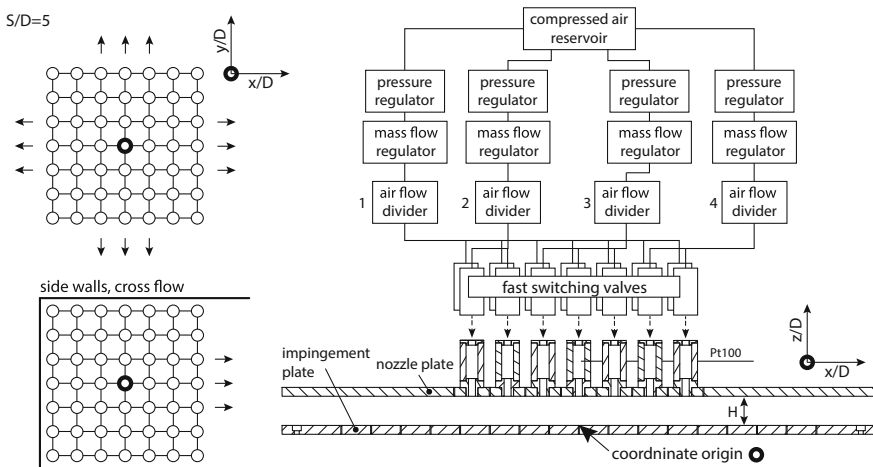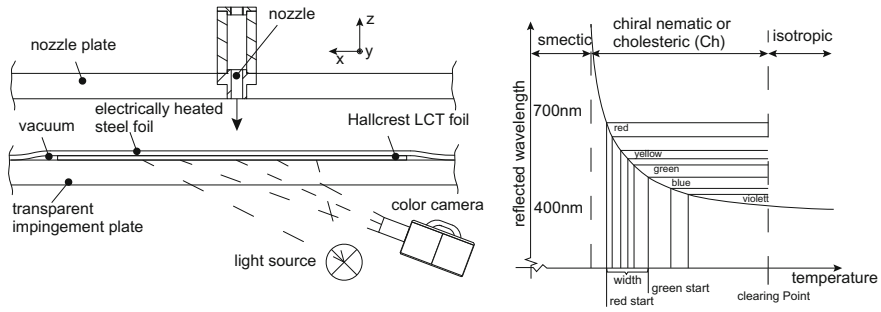

Fig. 1 Jet nozzle arrangement and compressed air supply

Fig. 2 Experimental setup. *Left* Schematic LCT assembly. *Right* Correlation between reflected wavelength and temperature response of thermochromic liquid crystals, [13]

$0.6 \, \text{m} \times 0.6 \, \text{m} \times 0.05 \, \text{mm}$. The range of measurable temperature is between 30° C and 46° C. Thereby, the colour play starts with red (cold) and changes over green to blue and violet (hot). If the temperature range is exceeded, the LCT foil appears constantly black and temperature information is not detectable. The measurement uncertainty for this specific LCT foil without calibration is as follows: start red and start green $T_{LCT} < 30°$ C, $\Delta T = \pm 0.5$ K, start blue $T_{LCT} > 35°$ C, $\Delta T = \pm 1$ K. In order to minimize the measurement inaccuracy of the LCT foil, a colour calibration against the Pt100 measurement technique is performed, which results in a reduced uncertainty of $\Delta T = \pm 0.1$ K.

The blank side of the steel foil is directed to the impinging jets while the visible side of the LCT foil is oriented to the transparent impingement plate. In order to fix the LCT assembly on the glass plate, the edges are sealed and a vacuum is applied to press the laminate together. The steel foil is connected to a power supply with a maximum electrical output of $P_{max} = 1000$ W. Controlling the electrical current, the steel foil can be heated continuously until a thermal equilibrium is obtained. The determination of wattage underlies an uncertainty of $\Delta P = \pm 0.065$ W. Simultaneously, the impinging jets are cooling the steel foil. Due to the resulting wall heat flux, the LCT foil is influenced thermally as well and a temperature depending colour distribution appears.

The electrical energy is adjusted for each operating point, which is defined by Reynolds number Re_D and temperature range of LCT foil. Depending on the resulting local wall temperatures, the liquid crystals reflect specific wave lengths of the light source through the glass plate back to a colour camera. These wave lengths are read out from the camera sensor as RGB values. In a post process these RGB values are converted in values of Hue, saturation and intensity. In order to complete this temperature measurement technique, a geometrical calibration is necessary for dewarping and allocating the real quasi wall temperatures.

For determination of Nusselt number distribution on the impingement plate assembly, it is assumed that the measured electrical power is equivalent to the emitted heat flux over the given heated area. Furthermore, in this consideration the heat conduction into the adjacent wall structure as well as radiation effects are neglected,

which is a first estimation. Hence, the wall heat flux is transferred completely into the cooling air mass flow of the impinging jets. The local Nusselt numbers are calculated as follows:

$$Nu_D = \frac{\dot{q}}{T_W - T_D} \cdot \frac{D}{\lambda_{air}} = \frac{P}{A_{heat} \cdot (T_W - T_D)} \cdot \frac{D}{\lambda_{air}} \tag{1}$$

Considering all measurement inaccuracies of the different involved measurement techniques, the uncertainty of the calculated Nusselt number can be determined as $\Delta Nu_D / Nu_D = 3 - 8\%$.

3 Results

The experimental study was focused on determining the combined influence of a dynamically forced 7 by 7 impinging jet array and a side wall induced crossflow on the local convective heat transfer. Therefore, the local temperature distribution was determined for cases with natural and directed crossflow by means of TLC-measurements. Post-processing of the raw data offered the possibility to convert the temperature distributions into local Nusselt number-distributions, which allows the quantification of the local forced convective heat transfer. The experimental data was obtained for a fixed impingement distance of $H/D = 5$ and a range of Reynolds numbers between $Re_D = 2150$ and $Re_D = 8300$.

The first phase of the study was the characterisation of the used impingement jet array. Therefore, the method of computation presented by Florschuetz et al. [2] was employed to validate the acquired data.

$$\overline{Nu}_1 = (x_n/D)^{-0.554} \cdot (y_n/D)^{-0.422} \cdot (z/D)^{0.068} \cdot Re_D^{0.727} \cdot Pr^{1/3} \tag{2}$$

It is only possible to compare experimental data to the presented equation, if the entire jet flow is constrained to exit in a single direction along the channel formed by the nozzle plate, the impingement surface and the side walls. If this is the case, the computed heat transfer coefficients are equivalent to the measured heat transfer coefficients resolved to one streamwise hole spacing ($\overline{Nu}_1$). To be more precise, $\overline{Nu}_1$ equals the mean value of the Nusselt number at the first upstream spanwise row of nozzles. Figure 3a shows the computed and measured value of $\overline{Nu}_1$ as a function of the Reynolds number. It is evident that the gradient for both cases is identical, if the Reynolds number is above $Re_D = 6000$. For Reynolds numbers below $Re_D = 6000$ the graphs are converging until they reach a point of intersection at a Reynolds number of $Re_D = 3100$. If the Reynolds number is even more decreased, the general trend of the graphs is conversed. For Reynolds numbers above the intersection, the experimental determined Nusselt number is always below the computed data. The deviation reaches its peak at a value of $\Delta \overline{Nu}_1 = 7.5$ for a Reynolds number of $Re_D =$
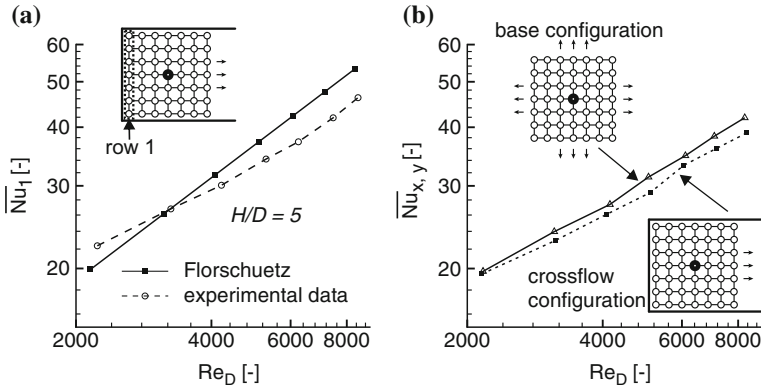
Fig. 3 **a** Comparison between computed an measured heat transfer coefficient $\overline{Nu}_1$. **b** Base configuration compared to crossflow configuration: Nusselt number as a function of the Reynolds number

6200. This comparison shows that the basic characteristic of the used testing rig is comparable to the computed approximation of Florschuetz, especially for higher Reynolds numbers. Therefore, it is possible to use the presented experimental set-up to acquire plausible data.

The second phase of the study was focused on the determination of the effects on the local heat transfer induced by directed crossflow. Therefore, the mean Nusselt number for the entire flow field $\overline{Nu}_{x,y}$ was calculated and linked to the variation of the Reynolds number. Figure 3b displays the dependency of the heat transfer from the Reynolds number. It is evident that the heat transfer for a Reynolds number of $Re_D = 2000$ is nearly the same for both cases. In case of the base configuration the heat transfer is characterized by a Nusselt number of $\overline{Nu}_{x,y} = 19.6$. In comparison, the crossflow case shows a Nusselt number of $\overline{Nu}_{x,y} = 19.8$. In both cases it is evident that the gradient of the Nusselt number is linear increased with the Reynolds number. In direct comparison of the base configuration and the crossflow configuration, it is noticeable that the values of $\overline{Nu}_{x,y}$ are divergent. The disparity is in the order of $\Delta\overline{Nu}_{x,y} = 3.2$ for an Reynolds number of $Re_D = 8100$. To clarify the origin of the disparity, it is necessary to analyze the crossflow oriented spatial development (x/D) of the Nusselt number $(\overline{Nu}_y)$. This particular Nusselt number is the average value at right angles to the crossflow on every position x in crossflow direction. Figure 4 exemplarily displays the spatial development for the Reynolds numbers $Re_D = 2150$, $Re_D = 4100$, $Re_D = 6100$ and $Re_D = 8300$. In case of the base configuration the spatial development for every Reynolds number is uniform. Only the maximum value of $\overline{Nu}_y$ is, as shown in Fig. 4a, steadily increased in dependancy to the Reynolds number. The same dependancy is evident in case of the crossflow configuration. Opposed to the base configuration the spatial development for every Reynolds number is not uniform. The development indicates a reduced heat transfer in dependency of the spatial position and, therefore, in dependency of the crossflow-velocity (u_{cf}). The
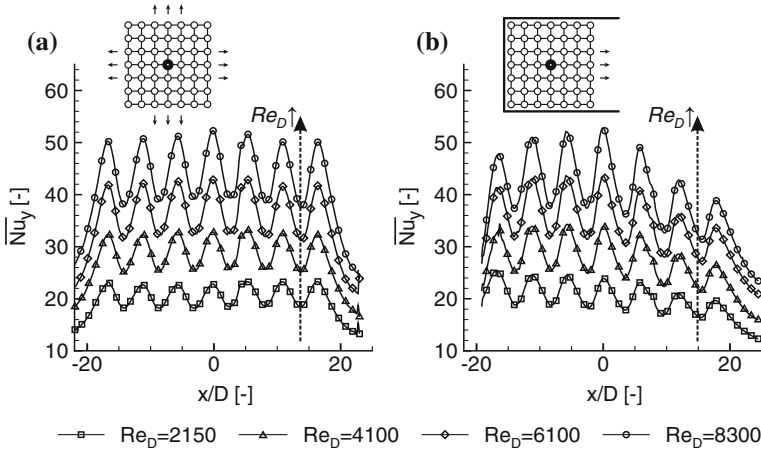
Fig. 4 Spatial development of the Nusselt number in crossflow direction (x/D): **a** Base configuration **b** Crossflow configuration

**Table 1** Reduced convective heat transfer in dependency of spatial position

Re_D	$\overline{Nu}_{y,R4}$	$\Delta\overline{Nu}_{R5}$ %	$\Delta\overline{Nu}_{R6}$ %	$\Delta\overline{Nu}_{R7}$ %
2150	23.7	2.5	11.7	16.8
4100	33.8	5.0	15.4	21.6
6100	43.4	5.9	16.4	22.6
8300	52.8	7.2	18.9	26.5

velocity increases steadily with every streamwise row of nozzles until the maximum is reached at the exit of the crossflow-channel. Table 1 illustrates the percental deprivation of the Nusselt number for every streamwise row of nozzles after the centerline $(R_5, R_6$ and $R_7)$ in relation to the Nusselt number directly under the centerline $\overline{Nu}_{y,R4}$. On the basis of the data it is evident that the crossflow induced deprivation of the Nusselt number is increased with the Reynolds number and the crossflow-velocity.

The approach to counter the Nusselt number deprivation is to use dynamically forced impingement jets. For a showcase Reynolds number of $Re_D = 7500$ the impingement frequency is varied between 0 and 500 Hz. The duty cycle is set to $DC = 50\%$ and the mass flow is the same as in case of steady blowing. Figure 5 displays the standardized excitation frequency (Sr_D) depending alteration of the Nusselt number due to dynamic forcing. It is evident that the convective heat transfer and, therefore, the Nusselt number is instantly increased if an excitation frequency is used. In case of the baseflow configuration for an frequency range of 0–0.12 a steady increase of the Nusselt number is recognizable. The maximum of the Nusselt number is located at an excitation frequency of $Sr_D = 0.12$ and is around 22% higher than the steady blowing case. If the frequency is further increased, the benefit of the Nusselt number is decreased to 19% and shows a nearly constant value for every frequency
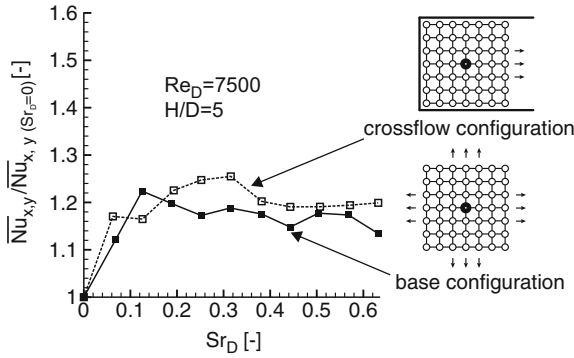
Fig. 5 Nusselt number benefit through dynamic forcing. $Re_D = 7500$, $H/D = 5$
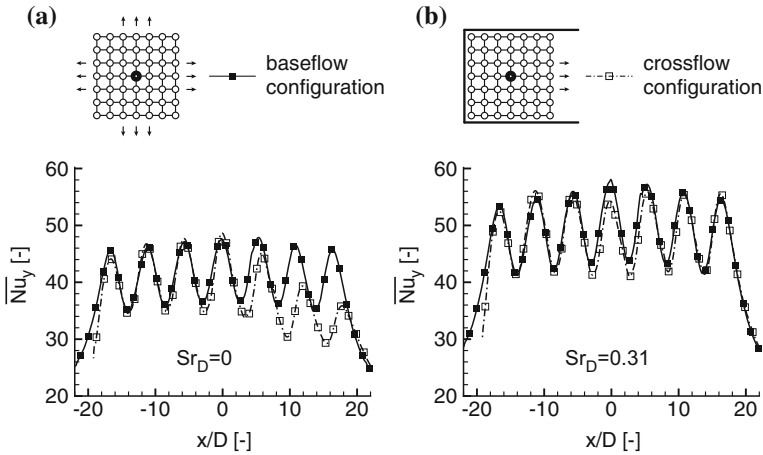
Fig. 6 Cancellation of the crossflow effect caused by dynamic forcing: **a** steady blowing **b** pulsed blowing

higher than $Sr_D = 0.2$. If the crossflow configuration is the subject matter, nearly the same trends are visible, but the maximum Nusselt number is located at an excitation frequency of $Sr_D = 0.31$ and is around 26.5% higher than the steady blowing case. If the excitation frequency is further increased the Nusselt number decreases to an almost constant level, which is around 20% higher than the steady blowing case.

All the results based on Fig. 5 are presented in relation to the individual steady blowing case and implicate a better improvement of convective heat transfer through dynamic impingement in case of the crossflow configuration. To better understand the improvement, it is necessary to take a closer look on crossflow oriented spatial development of the Nusselt number. Figure 6a displays the spatial development for both configurations in case of steady blowing. The other figure shows both configurations in case of dynamic impingment with an Strouhal number of $Sr_D = 0.31$,

which equals the optimal set of parameters presented in Fig. 5. In case of steady blowing, it is re-assessedly evident that the crossflow induced deprivation of the Nusselt number is increased with the crossflow-velocity. In case of dynamic impingement, the displayed data shows a completely different behaviour. Both spatial developments are nearly superimposable, therefore, the negative effects of the crossflow are entirely extinguished. In accordance to the results based on Fig. 5 the absolut increase of the Nusselt number is $\Delta \overline{Nu}_{x,y}/\overline{Nu}_{x,y(Sr_D=0)} = 19\%$. The cancelling of the crossflow effect is based on the pulsation of the cooling fluid because the duty cycle of $DC = 50\%$ results in a doubling of the peak jet velocity and thus in a quadruplication of the peak jet-impulse. Thereby, strong vortex rings are created, which are increasing the penetration depth of the cooling fluid. Therefore, the vortex rings are able to transport more cooling fluid directly to the impingement plate to increase the cooling efficiency. The data also implies that the maximum Nusselt numbers that can be reached are these of the base configuration at a specific frequency. Therefore, the dynamic forcing allows the complete elimination of the crossflow based Nusselt number deprivation.

4   Conclusions

The study was focused on detailed heat transfer investigations of a 7 by 7 jet array impinging on a hot surface. Thereby, the influence of directed crossflow induced by side walls was compared to the natural crossflow case without channelling. Pulsed blowing was employed to enhance local convective heat transfer and to compensate the Nusselt number reducing effect of crossflow. Liquid crystal thermography was employed to determine the local wall temperature and therefore to compute the local Nusselt number. The first part of the study was focused on the dependency between Reynolds number and Nusselt number and the resulting differences in case of directed crossflow. The main subject of the second part was to investigate the influence of dynamically forced impinging jets on the same experimental configurations. In both cases the results show that the local Nusselt number is steadily increased with the Reynolds number. Furthermore, it is evident that the deviation between both cases is increased with the Reynolds number as well. Therefore, the Nusselt number is decreased if the crossflow-velocity is increased. If the excitation frequency is varied, the resulting Nusselt number can be increased. In case of natural crossflow the maximum gain is around $\Delta \overline{Nu}_D/\overline{Nu}_{D(Sr_D=0)} = 22\%$ at a Strouhal number of $Sr_D = 0.12$. For directed crossflow the gain is even 4% higher at a Strouhal number of $Sr_D = 0.31$. In both cases the increase of the Nusselt number after the most effective Strouhal number is constant if the Strouhal number is further increased. A closer contemplation of the results show that the natural crossflow case always presents the maximal attainable Nusselt number. Therefore, it is evident that the dynamically forcing of the impinging jets is countering the deprivation effects induced by directed crossflow. Considering all the results, it is necessary to further investigate the mecha-

nisms, that counter the deprivation effects. Thus, the researched frequency variation has to be extended and the dependency of the impingement distance has to be taken into account.

References

1. Florschuetz, L.W., Metzger, D.E., Takeuchi, D., Berry, R.: Multziple Jet Impingement Heat Transfer Characteristic—Experimental Investigation of In-Line and Staggered Arrays With Crossflow. NASA-CR-3217. Arizona State University, Tempe, Department of Mechanicle Engineering (1980)
2. Florschuetz, L.W., Truman, C.R., Metzger, D.E.: Streamwise flow and heat transfer distributions for jet array impingement with crossflow. J. Heat Trans. **103**, 337–342 (1981)
3. Weigand, B., Spring, S.: Multiple jet impingement—A review. Heat Trans. Res. **42**(2), 101–142 (2010)
4. Xing, Y., Spring, S., Weigand, B.: Experimental and numerical investigation of heat transfer characteristics of inline and staggered arrays of impinging jets. J. Heat Trans. **132**, 92201/1–11 (2010)
5. Liu, T., Sullivan, J.P.: Heat transfer and flow structures in an excited circular impingement jet. Int. J. Heat Mass Trans. **39**, 3695–3706 (1996)
6. Vejrazka, J., Tihon, J., Marty, P., Sobolik, V.: Effect of an external excitation on the flow structure in a circular impinging jet. Phys. Fluids **17**, 3695–3706 (1996)
7. Hofmann, H.M., Movileanu, D.L., Kind, M., Martin, H.: Influence of a pulsation on heat transfer and flow structure in submerged impinging jets. Int. J. Heat Mass Trans. **50**, 3638–3648 (2007)
8. Gharib, M., Rambod, E., Shariff, K.: A universal time scale for vortex ring formation. J. Fluid Mech. **360**, 121–140 (1998)
9. Herwig, H., Middelberg, G.: The physics of unsteady jet impingement and its heat transfer performance. Acta Mech. **201**, 171–184 (2008)
10. Middelberg, G., Herwig, H.: Convective heat transfer under unsteady impinging jets: The effect of the shape of the unsteadiness. J. Heat Mass Trans. **45**, 1519–1532 (2009)
11. Janetzke, T.: Experimental investigations of flow field and heat transfer characteristics due to periodically pulsating impinging air jets. Heat Mass Trans. **45**, 193–206 (2008)
12. Haucke, F., Nitsche, W., Wilke, R., Sesterhenn, J.L.: Experimental and numerical investigation regarding pulsed imipingement cooling. Deutscher Luft- und Raumfahrt Kongress Rostock (2015)
13. Stasiek, J.: Thermochromic liquid crystals and true colour image processing in heat transfer and fluid—Flow research. Heat Mass Trans. **33**, 27–39 (1997)